Desalination and Water Treatment
www.deswater.com

doi: 10.5004/dwt.2017.20119

62 (2017) 257–266
February

Characteristics of cerium-aluminum-manganese mixed oxides and their performance in adsorbing methyl violet dye from an aqueous solution

Piaw Phatai[a,*], Cybelle Morales Futalan[b,†]

[a]*Department of Chemistry & Polymer and Material Research Groups, Faculty of Science, Udon Thani Rajabhat University, Udon Thani, 41000 Thailand, Tel. +66 42 211 040 Ext. 201-3; Fax: +66 42 341 614-5; email: piawtee99@hotmail.com*
[b]*Environment Business Line, Aecom Philippines Consultant Corporation, Taguig, Philippines 1634, Tel. +63 24 785 854; email: cmfutalan@gmail.com*

Received 3 August 2015; Accepted 6 August 2016

ABSTRACT

In this work, CeAl and $CeAlMn_x$ oxides ($x = 0.1$, 0.3, 0.5 and 0.7) were prepared using a co-precipitation method and their use for removal of methyl violet dye from an aqueous solution was investigated. The characteristics of the mixed oxides were determined using XRD, FT-IR, UV-vis DRS, SEM and EDX. It was found that cerium, aluminum and manganese ions were homogeneously incorporated into the cubic fluorite structure of CeO_2. Moreover, the mixed oxides were found to consist of small grains containing pores, which resulted in a large surface area to volume ratio. Batch adsorption studies were performed to determine the contact time required to achieve equilibrium. The removal of dye by CeAl and $CeAlMn_x$ ($x = 0.1$ and 0.3) attained equilibrium after 60 min, while oxide samples with higher manganese fractions achieved equilibrium in 120 to 150 min. Based on the isotherm data, the adsorption behavior of CeAl was found to follow a Langmuir isotherm ($R^2 = 0.9951$) with a maximum adsorptive capacity of 2.35 mg/g. Results show that the Freundlich model best describes the adsorption of MV dye onto all $CeAlMn_x$ formulations.

Keywords: Cerium and aluminum mixed oxides; Langmuir isotherm; Freundlich isotherm; Temkin isotherm; Manganese; Methyl violet dye

1. Introduction

Methyl violet (MV) dye ($C_{24}H_{28}ClN_3$), otherwise known as the hydrochloride of pentamethyl triamino triphenyl carbinol, is commonly used for dyeing cotton, wood, paper and silk and for manufacturing carbon paper, copying pencils, stamping ink and other colored materials. It is often present in the effluents produced by the textile, paper, printing, food and cosmetics industries [1]. Dyes are characterized by their stability due to the complex aromatic structure that makes them difficult to remove. Apart from being unaesthetic, the presence of dyes in water reduces light penetration, which hinders photosynthesis in aquatic plants. Moreover, dyes are known to cause allergic reactions in some people and some are considered carcinogenic [2]. It is therefore essential to treat dye-contained effluents prior to their discharge.

Conventional approaches used in dye removal are ultra-filtration [3], extraction [4], oxidation with ozone [5], reaction with hydrogen peroxide [6] and adsorption [7,8]. Among these technologies, adsorption has been considered an attractive method because it has several advantages including high efficiency, ease of operation, low cost, simplicity of design, insensitivity to toxic pollutants and reduced production of harmful substances [9]. Different porous adsorbents including ceramics [10], agricultural wastes [11], fly ash [12], perlite [13] and mixed oxides [7,14,15] have been investigated for their effectiveness in

---

* Corresponding author.

† Cybelle Morales Futalan (Co-Author).

1944-3994/1944-3986

adsorptive removal of dyes from aqueous solutions. The efficiencies of these adsorbents vary, but high cost generally limits their commercial application.

Mixed metal oxides typically consist of two or more cations with different oxidation states, ionic radii and coordination numbers. This diversity presents an opportunity to generate materials with physical and chemical properties that differ from those of simple metal oxides [16]. Mixed oxides such as Fe-Al [14], Al-Co [15], Co-Ni [16], Fe-Sn [17], Ni-Zn [18] and Fe-Mn [19] have been used for dye removal. Ce and Al mixed oxides have been used as heterogeneous catalysts and adsorbents due to their large surface area to volume ratio and high catalytic/adsorptive performance. In previous work [7] Ce_xAl_{1-x} (x = 0.3, 0.5 and 0.7) mixed oxides were assessed for their capacity to adsorb MV dye. It was found that $Ce_{0.3}Al_{0.7}$ with its rough texture and high surface to volume ratio provided the best adsorption efficiency at pH 9.0, a contact time of 120 min and a shaking speed of 150 rpm. This study incorporated manganese ions into a $Ce_{0.3}Al_{0.7}$ oxide host as ternary mixed oxides for the purpose of determining whether this increases MV adsorption from aqueous solutions by CeAl mixed oxides. The ternary mixed oxides of Fe-Al-Cr [20] and Fe-Al-Ce [21] have previously been investigated for their capacity to adsorb fluoride ions from aqueous solutions. However, the new ternary mixed oxides of $CeAlMn_x$ prepared by a co-precipitation method have not been studied for the removal of dyes from an aqueous solution.

The structural and chemical properties of the adsorbents were determined using X-ray diffraction (XRD), Fourier transform infrared spectroscopy (FT-IR), diffuse reflectance UV-vis spectroscopy (UV-vis DRS), scanning electron microscopy (SEM) and energy dispersive X-ray spectroscopy (EDX). The removal of MV dye by adsorption onto $Ce_{0.3}Al_{0.7}$ and $Ce_{0.3}Al_{0.7}Mn_x$ (x = 0.1, 0.3, 0.5 and 0.7) oxides was studied by varying the contact time and the initial dye concentration. Langmuir, Freundlich and Temkin isotherms were employed to determine the adsorption mechanisms. This information may stimulate further efforts to develop practical applications of these mixed oxides to remove MV dye from wastewater.

2. Materials and methods

2.1. Materials

All chemicals used were of analytical grade. $Ce(NO_3)_3{\cdot}6H_2O$, $Al_2(SO_4)_3{\cdot}18H_2O$, $MnSO_4{\cdot}H_2O$, polyethylene glycol (PEG, MW = 20,000), NH_4OH, $n\text{-}C_4H_9OH$, KH_2PO_4, KOH, $NaH_2PO_4{\cdot}H_2O$, Na_2HPO_4, H_3PO_4, H_3BO_3 and NaOH were obtained from Sigma-Aldrich. MV dye with a MW = 393.95 (Fig. 1) was purchased from Sigma-Aldrich and used without additional purification. Stock solutions of MV dye were prepared by dissolving a precise amount of MV dye in distilled water and buffering the solution to pH 9.0 (European Pharmacopoeia 5.0, 2012).

2.2. Preparation of adsorbents

$Ce_{0.3}Al_{0.7}$ and $Ce_{0.3}Al_{0.7}Mn_x$ (x = 0.1, 0.3, 0.5 and 0.7) oxides were prepared using a co-precipitation method modified from Chen et al. [22]. The precursors, $Ce(NO_3)_3{\cdot}6H_2O$, $Al_2(SO_4)_3{\cdot}18H_2O$, and $MnSO_4{\cdot}H_2O$ were dissolved in the desired molar ratio in water and mixed with constant stirring. About 1.0 g PEG was added under vigorous stirring to the precursor solution as a template, followed by dropwise addition of NH_4OH to the mixture until pH 9.0 was attained. Each solution was chilled to 0°C for 24 h, filtered and repeatedly washed with n-butyl alcohol to remove any un-reacted species. The samples were dried in an oven at 120°C for 2 h, and then the dried samples were calcined in air at 600°C for 4 h. $Ce_{0.3}Al_{0.7}$ will hereafter be referred to as CeAl and compounds of $Ce_{0.3}Al_{0.7}Mn_x$ (x = 0.1, 0.3, 0.5 and 0.7) will be referred to as $CeAlMn_{0.1}$, $CeAlMn_{0.3}$, $CeAlMn_{0.5}$ and $CeAlMn_{0.7}$, respectively.

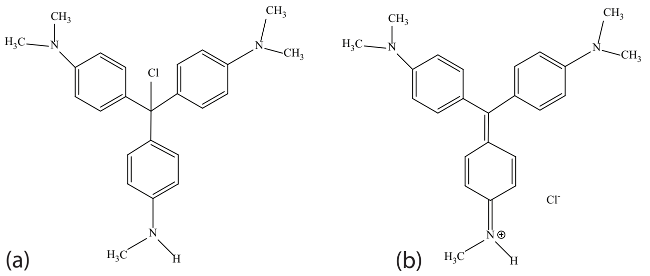

Fig. 1. Structure of methyl violet dye before (a) and after (b) dissolution.

2.3. Equipment

The pH measurements were performed using a pH meter (Consort C830, Belgium). An electronic balance (Mettler Toledo AL204) with an accuracy of 0.0001 g was used for precisely weighing all chemicals. An orbital shaker bath (VS-202P, AC220V, 50 Hz) was utilized in all adsorption experiments. Quantitative analysis of the concentration of MV dye was performed using a UV-vis spectrophotometer (Hitachi U-2900).

The phases of the cerium, aluminum and manganese oxides were determined using X-ray diffraction (XRD, Bruker D8 ADVANCE Series 2). The unit was equipped with a Cu tube (K_α wavelength = 0.15406 nm) operating at 40 kV and 40 mA. The FT-IR spectra of fresh and spent mixed oxides were determined by Fourier Transform Infrared Spectroscopy (FT-IR, Spectrum Two-Perkin Elmer) in the range of 4,000–500 cm^{-1}. To study the coordination and oxidation states of the metal ions, diffuse reflectance UV-vis spectra (UV-vis DRS) were measured at room temperature using a Lamda 35, Perkin Elmer system equipped with a reflectance attachment containing a $BaSO_4$ coated integration sphere. The surface morphology was examined using scanning electron microscopy (SEM, Hitachi S-3000N) with an accelerating voltage of 5 kV. In preparation for the SEM observations, the sample surfaces were made conductive by sputter coating them with gold for 5 min using a K500X sputter coater operating at a pressure of 9×10^{-2} mbar and a current of 20 mA. The elemental composition of the mixed oxides was measured using Energy Dispersive X-ray Spectroscopy (EDX, Hitachi S-3000N).

2.4. Batch adsorption studies

Batch experiments to measure the adsorption of MV dye by CeAl and $CeAlMn_x$ mixed oxides were performed in two ways. The first was as a function of contact time (15–180 min) to establish the experimental times required to ensure the adsorption process continued to completion. For these experiments, the initial dye concentration was 3 mg/L. Exactly 25 mL of this dye solution was added to a 250 mL Erlenmeyer flask with 0.10 g of the adsorbent material. The solution was agitated at a constant speed of 150 rpm and the pH was held constant at 9.0 by the buffered solution. At times between 15 and 180 min, the adsorption process was interrupted and the mixture was filtered using Whatman-42 filter paper. The clear filtrates were diluted and then analyzed for residual MV dye concentration using VIS spectrophotometry at a wavelength of 584 nm. The adsorption capacity of the MV dye was calculated as:

$$\text{Adsorption capacity (mg/g)} = \frac{(C_i - C_t)V}{m} \qquad (1)$$

where C_i and C_t are the initial and equilibrium dye concentrations (mg/L), respectively. V is the volume of the solution (L) and m is the mass of metal oxide adsorbent (g) initially added.

The isotherm experiments were conducted following process similar to the one above, however the time-dependent experiments had established that it was only necessary to continue the adsorption process for 120 min before equilibrium could be assured in of 3 mg/L MV dye solutions. For higher concentrations used in the isotherm experiments, the equilibrium time was expected to be shorter. MV dye solutions (pH 9.0) with initial concentrations ranging from 5 to 50 mg/L were used. The MV dye remaining after adsorption (C_e, mg/L) was measured in the equilibrated solution. The equilibrium adsorption capacity (q_e, mg/g) was calculated using Eq. (1) with C_e substituted for C_t.

3. Results and discussion

3.1. Characterization of the mixed oxides

Fig. 2 shows the XRD patterns obtained from the CeAl and $CeAlMn_x$ mixed oxide samples of various compositions after calcination at 600°C for 4 h. The samples exhibited the typical single phase cubic fluorite structure of CeO_2 with peaks at 2θ angles of 28.7°, 33.2°, 47.4°, 56.0°, 69.0° and 76.0° corresponding to (111), (200), (220), (311), (400) and (331) crystal planes (JCPDS card number 34–394), respectively. The measured lattice parameter, 0.545 nm, agreed well with literature values [23]. The spectra collected from the $CeAlMn_x$ samples were similar to those obtained from the CeAl sample which suggests that the $CeAlMn_x$ oxide samples were not simple composites of the individual Ce, Al and Mn oxides. Rather, they were in the form of a CeO_2 solid solution with metal atoms embedded in its crystal structure. This is probably due to Al^{3+} (0.054 nm) and Mn^{3+} (0.062 nm) having smaller ionic radii compared to those of Ce^{4+} (0.097 nm) and Ce^{3+} (0.114 nm) [24] allowing them to be readily substituted for Ce atoms in the lattice. Insertion of Al^{3+} and Mn^{3+} into the CeO_2 lattice was also proposed by Xiaodong et al. [24].

Figs. 3(A) and (B) show the FT-IR spectra obtained from fresh (a–c) and spent adsorbents (d–f). In Fig. 3A (a–f), the absorption bands at approximately 3,200–3,700 cm^{-1} and ~1,673 cm^{-1} were present in all the FT-IR spectra and match the expected positions of M-OH stretching and bending vibrations, respectively. This indicates the presence of physisorbed water molecules in the samples due to the adsorption of atmospheric moisture during the measurements. The absorption band at ~1,151 cm^{-1} in Fig. 3A (a)–(c) is due to symmetric deformation vibrations of Al-O and S-O bonds [24,25]. In Fig. 3B (a)–(c), the bands at ~570–660 cm^{-1} are characteristic of metal-oxygen-metal vibrations [17,20] which appeared when manganese was added. The FT-IR results suggest that different atomic connectivities and associated vibrations were present in the CeAlMn mixed oxide samples. Figs. 3A and B (d–f) show FT-IR spectra obtained from spent $CeAlMn_x$. The absorption band at ~1,300–1,500 cm^{-1} arose from bending vibrations of the methyl and methylene groups in the methyl violet dye [26], confirming the presence of the adsorbed dye molecules. The weakening of the Al-O and S-O stretching bond features in Fig. 3(A) is consistent with the adsorbent being covered with MV dye molecules, as is the weakening of the M-O-M vibration modes apparent in Fig. 3(B).

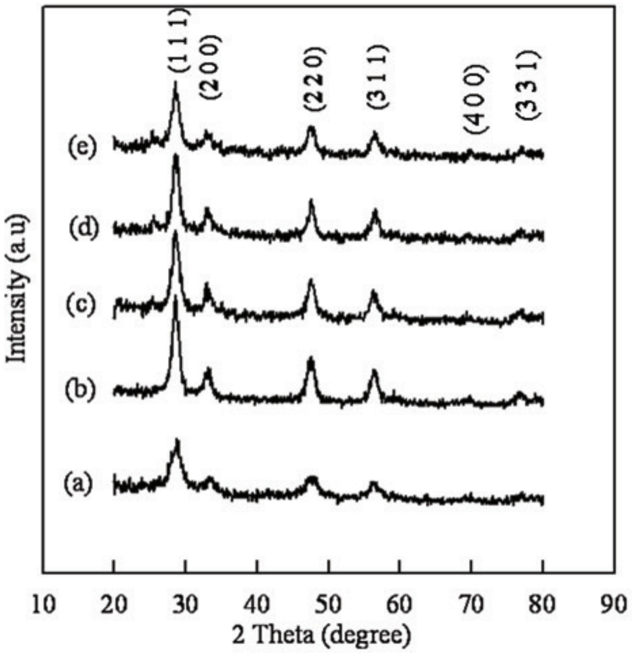

Fig. 2. XRD patterns obtained from mixed oxides (a) CeAl, (b) $CeAlMn_{0.1}$, (c) $CeAlMn_{0.3}$, (d) $CeAlMn_{0.5}$, and (e) $CeAlMn_{0.7}$.

UV-DR spectroscopy can yield information about the coordination environment and oxidation states of embedded transition and rare earth metal ions. Fig. 4 shows UV-vis DRS spectra obtained from mixed oxide samples over the wavelengths of 200–800 nm. Peaks at ~265 and 320 nm are related to the charge transfer transitions of $O^{2-} \rightarrow Ce^{3+}$ and $O^{2-} \rightarrow Ce^{4+}$ respectively [27,28]. This suggests that Ce^{3+} and Ce^{4+} ions coexist within the mixed oxide lattices.

Fig. 5 shows SEM micrographs taken at a magnification of 15,000x for various compositions of fresh CeAl and $CeAlMn_x$ powder samples following calcination. It can be seen that the oxide morphologies consisted of a range of fine grain sizes separated by an extensive network of pores.

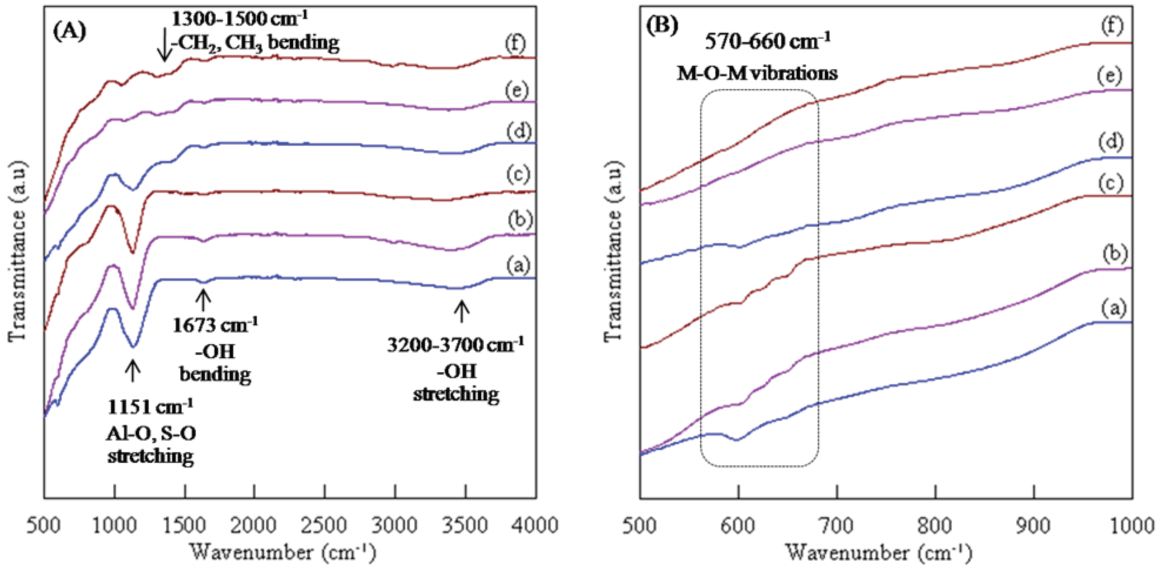

Fig. 3. FT-IR spectra of fresh mixed oxides: (a) CeAl, (b) $CeAlMn_{0.3}$, (c) $CeAlMn_{0.7}$, and spent mixed oxides: (d) CeAl, (e) $CeAlMn_{0.3}$, (f) $CeAlMn_{0.7}$ at the wavenumbers of (A) 500–4000 cm^{-1} and (B) 500–1000 cm^{-1}.

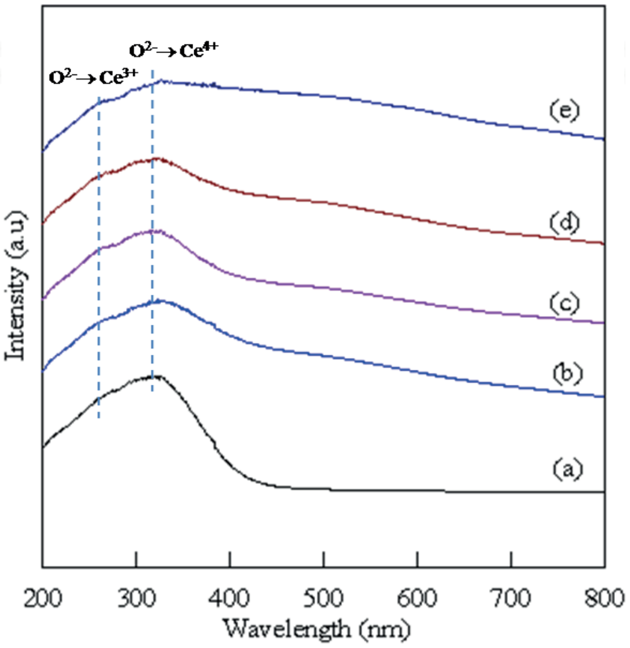

Fig. 4. UV-vis DRS spectra obtained from mixed oxides (a) CeAl, (b) $CeAlMn_{0.1}$, (c) $CeAlMn_{0.3}$, (d) $CeAlMn_{0.5}$, and (e) $CeAlMn_{0.7}$.

This high surface area to volume morphology would appear to have facilitated adsorption of MV dye molecules.

The chemical composition of the oxides studied was determined by means of large area EDX analysis. These results are shown in Table 1. The measured oxygen weight fractions are more than double the 34% to 36% expected values. This was almost certainly a result of atmospheric contamination by oxygen and water vapour. This contamination depressed the weight fractions of Ce, Al and Mn and so these figures cannot be considered reliable. It is notable that if the stoichiometry of the mixed oxide materials were as the EDX results suggest, it would have been impossible to obtain powder diffraction spectra yielding a lattice parameter, 0.545 nm, in agreement with the literature value. The measured weight percentages of cerium, aluminum and manganese were 3%–5%, 10%–15% and 0%–5%, respectively. The expected weight percentages for these metals were 14%–45%, 6%–20% and 0%–43%. So, the Ce levels are a factor of about nine lower than expected. Al levels were similar to those expected, but lower values were about 50% higher than expected. Mn levels were about a factor of five lower than expected. Apart from the problem with oxygen contamination, these discrepancies could have been exacerbated by metal loss during template removal. A similar result was reported by Zabilskiy et al. [29] who, in preparing $CuO-CeO_2$ catalysts for N_2O decomposition studies, noticed NaOH leaching during template removal resulted in a minor loss of CuO.

Table 1 shows that sulfur was detected in all adsorbents at weight percentages between about 2% and 5%. The true weight percentages were almost certainly much higher due to oxygen contamination lowering the measured values for the other elements. This contamination must have originated from the precursors, $Al_2(SO_4)_3 \cdot 18H_2O$ and $MnSO_4 \cdot H_2O$ used in the preparation of the adsorbent. Clearly the sulfur was not eliminated as a result of calcination at 600°C for 4 h. Xiaodong et al. [24] reported that chemisorbed SO_2 or other sulfate species contained in MnO_x–CeO_2-Al_2O_3 catalysts were only removed after calcination for 30 min in air at 800°C. However, such a high calcination temperature caused sintering of the metal oxides, thus decreasing their catalytic activity. The presence of sulfur may have "poisoned" surface sites, thus reducing the adsorption efficiency of all the mixed oxides investigated. Judging from the EDX results, this effect was reasonably uniform in all samples. However the effect of site "poisoning" is not likely to change the adsorption mechanisms at play during the adsorption of MV dye. Rather it will limit the efficiency of the process and the evidence for this will be discussed in Section 3.5.

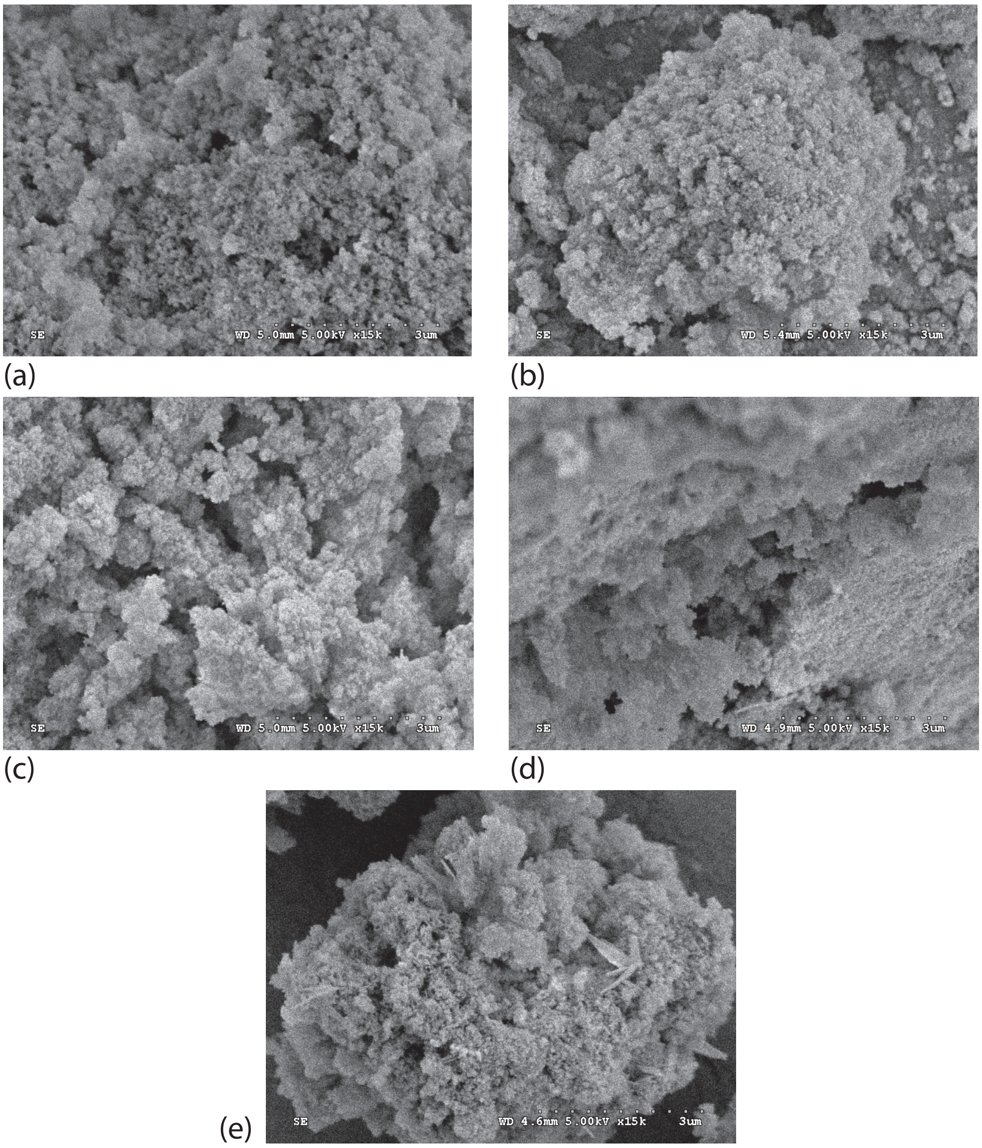

Fig. 5. SEM images of mixed oxides at 15,000 × magnification (a) CeAl, (b) $CeAlMn_{0.1}$, (c) $CeAlMn_{0.3}$, (d) $CeAlMn_{0.5}$, and (e) $CeAlMn_{0.7}$.

Table 1
Weight percentages of Ce, Al, Mn, O and S in mixed oxides derived from the EDX measurements. The shells to which electrons transition are shown for each element

Adsorbents	% weight				
	Ce (L)	Al (K)	Mn (K)	O (K)	S (K)
CeAl	4.49	14.77	0.00	75.54	5.20
$CeAlMn_{0.1}$	4.93	14.85	0.99	76.95	2.28
$CeAlMn_{0.3}$	3.51	13.04	2.15	77.81	3.48
$CeAlMn_{0.5}$	3.62	13.34	3.74	76.08	3.21
$CeAlMn_{0.7}$	3.15	10.57	4.52	77.59	4.16

3.2. The effect of contact time

The equilibrium time required for the maximum adsorption of MV dye onto CeAl and $CeAlMn_x$ oxides was established by performing a series of adsorption experiments with contact times between 15 and 180 min. The amounts of MV dye removed from aqueous solutions by CeAl and $CeAlMn_x$ are plotted in Fig. 6 as functions of time. The adsorption capacities of CeAl, $CeAlMn_{0.1}$ and $CeAlMn_{0.3}$ increased rapidly in the first 15 min, while $CeAlMn_{0.5}$ and $CeAlMn_{0.7}$ increasing more gradually. The adsorption capacities of CeAlMn$_{0.5}$ and CeAlMn$_{0.7}$ gradually increased for up to 120 min, reaching maximums of 0.37 and 0.33 mg/g, respectively. The highest adsorption capacity of about 0.5 mg/g was measured for the CeAlMn$_{0.1}$ oxide. Within experimental error, it was apparent from these measurements that the adsorption process had reached equilibrium well before 180 min, so subsequent experiments exposed the mixed oxides to MV dye solutions for 120 min.

3.3. The effect of initial dye concentration

Initial dye concentration was expected to be one of the most important experimental parameters driving the transfer of dye from the solution to an adsorbent. Experiments were performed at different initial MV dye concentrations ranging from 5 to 50 mg/L with an adsorbent dose of 0.1 g. The adsorption capacity of each of the mixed oxide materials investigated versus the initial concentration of MV dye is shown in Table 2 and plotted in Fig. 7. The adsorption capacity of all adsorbents increased with increasing initial dye concentration since higher initial dye concentrations resulted in a larger concentration gradient between the solution and the adsorbent surface. Similar results were found for the adsorption of Congo red onto MFe$_2$O$_4$ (M = Mn, Fe, Co, Ni) by Wang et al. [30].

3.4. Adsorption isotherm modeling

It is relevant to describe how adsorbed molecules are distributed between the liquid and solid phases when the adsorption process has reached its equilibrium state.

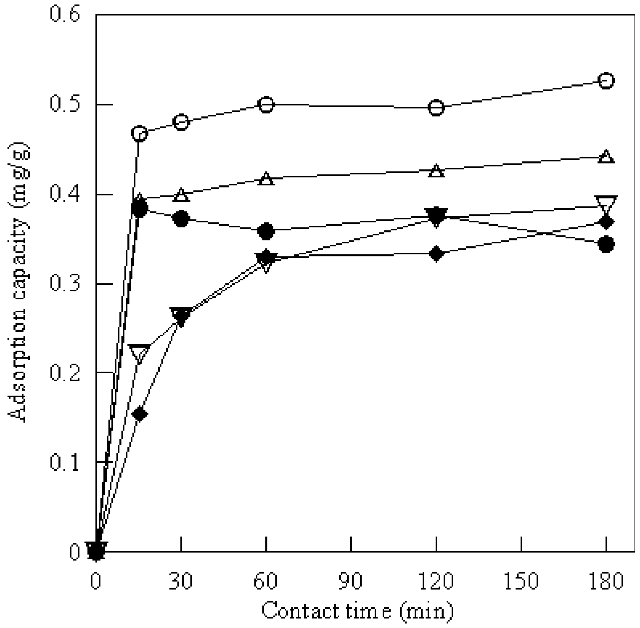

Fig. 6. The effect of contact time on adsorption capacity by mixed oxides: (•) CeAl, (○) CeAlMn$_{0.1}$, (Δ) CeAlMn$_{0.3}$, (∇) CeAlMn$_{0.5}$ and (♦) CeAlMn$_{0.7}$ (adsorbent dose = 0.10 g; initial dye concentration = 3.0 mg/L; pH = 9.0, shaking speed = 150 rpm).

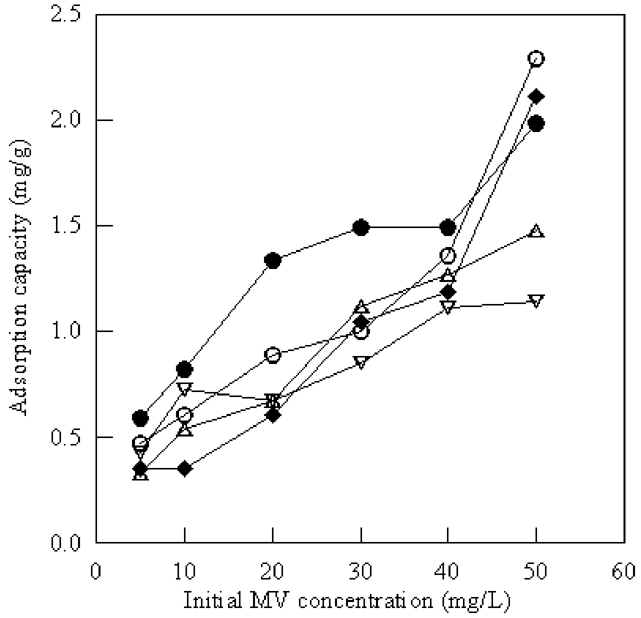

Fig. 7. The effect of initial dye concentration on adsorption capacity of mixed oxides: (•) CeAl, (○) CeAlMn$_{0.1}$, (Δ) CeAlMn$_{0.3}$, (∇) CeAlMn$_{0.5}$ and (♦) CeAlMn$_{0.7}$ (adsorbent dose = 0.10 g; pH = 9.0, shaking speed = 150 rpm).

Table 2
MV dye adsorption for all mixed oxide adsorbents and initial dye concentrations

Initial MV dye		MV amount adsorbed									
		CeAl		CeAlMn$_{0.1}$		CeAlMn$_{0.3}$		CeAlMn$_{0.5}$		CeAlMn$_{0.7}$	
Conc.(mg/L)	Amount(mg)	mg	%	mg	%	mg	%	mg	%	mg	%
5	0.125	0.100	80	0.089	71	0.078	62	0.081	65	0.070	56
10	0.25	0.205	82	0.180	72	0.134	53	0.175	70	0.157	63
20	0.5	0.387	77	0.353	71	0.314	63	0.367	73	0.317	63
30	0.75	0.585	78	0.483	64	0.502	67	0.554	74	0.501	67
40	1	0.886	89	0.608	61	0.638	64	0.674	67	0.594	59
50	1.25	0.833	67	0.774	62	0.755	60	0.795	64	0.706	56
Averages		0.499	79	0.414	67	0.403	62	0.441	69	0.391	61

The equilibrium data on the capacity of CeAl and CeAlMn$_x$ oxides to remove MV dye were analyzed using three isotherms, Langmuir, Freundlich and Temkin. The Langmuir isotherm is based on four assumptions, (i) that adsorption is limited to monolayer coverage, (ii) that all surface sites are alike and can only accommodate one adsorbed atom, (iii) that the ability of a molecule to be adsorbed on a given site is independent of occupancies of neighboring sites, and (iv) that adsorbed species can subsequently desorb [30–32]. The Langmuir equation expresses these assumptions in the form:

$$q_e = q_m \frac{K_L C_e}{1 + K_L C_e} \tag{2}$$

where C_e is the equilibrium concentration of the dye solution following adsorption (mg/L), q_e is the amount of dye adsorbed per unit mass of adsorbent (mg/g), q_m is the monolayer dye capacity on the adsorbent material (mg/g) and K_L is the adsorption equilibrium constant (L/mg) [33]. The Langmuir isotherm can be written in linear form as:

$$\frac{C_e}{q_e} = \frac{1}{q_m K_L} + \frac{C_e}{q_m} \tag{3}$$

and a plot of C_e/q_e vs. C_e yields values for the parameters, q_m and K_L.

The Freundlich isotherm is an empirical relationship explaining the adsorption of solutes from a liquid to a surface. It allows for different sites with different adsorption energies to be involved in the adsorption process [32,34–36] and the linear form of the Frendlich equation is:

$$\ln q_e = \ln K_F + \frac{1}{n} \ln C_e \tag{4}$$

where K_F (mg/g) and n are the Frendlich constants associated with adsorption capacity and adsorption intensity of the dye onto the adsorbent, respectively.

The Temkin isotherm assumes that the heat of adsorption decreases linearly as the adsorbate covers the binding sites. A linear form of the Temkin isotherm equation can be expressed as:

$$q_e = B \ln A + B \ln C_e \tag{5}$$

where B = RT/b and A is an equilibrium constant corresponding to the maximum binding energy (L/g). b is the Temkin constant related to the heat of adsorption (kJ/mol), R is the gas constant and T (K) is the absolute temperature [32]. All three adsorption isotherms were used in their linear forms, i.e., Eqs. (3)–(5) and the parameters were extracted from the respective plots as shown in Table 3.

The applicability of the respective isotherm equations was judged by the values of the R^2 correlation coefficients. The high R^2 value obtained for the Langmuir isotherm, when applied to the CeAl mixed oxide adsorbent data suggests that it may be appropriate in this case and yielded a q_m of 2.35 mg/g and a K_L of 0.31 L/mg. However, the Langmuir model was not successful in accounting for the data obtained from the manganese containing mixed oxides. This was best described by the more complex Freundlich model, suggesting multilayer adsorption with several types of active adsorption sites associated with different adsorption energies. The measured n values ranged from 1 to 2, indicating moderately difficult adsorption characteristics. The Temkin model was not as successful in describing any of the data. This suggests that adsorption of MV dye probably involved different sites and site energies with other possible complexities such as particle agglomeration.

3.5. Comparison with previous studies

In Table 4, the adsorption capacity of CeAl in removing MV dye in the present study is compared with other adsorbents employed in previous work. The maximum q_m value measured in the current work was found when using CeAl as the adsorbent (2.35 mg/g). This was lower than that achieved previously with CeAl (25 mg/g) under similar experimental conditions [7]. In previous work, CeAl oxide was prepared using nitrate precursors for Ce and Al, whereas the CeAl and CeAlMn$_x$ prepared in this work used a nitrate precursor for Ce and sulfate precursors for Al and Mn. Sulfur present in the mixed oxide was not removed by calcination at 600°C and therefore may have formed sulfur oxide in the mixed oxide lattice. Sulfur may have blocked otherwise active sites from

Table 3
Isotherm model parameters obtained for MV adsorption onto CeAl and CeAlMn$_x$

Isotherms	Parameters	Adsorbents				
		CeAl	CeAlMn$_{0.1}$	CeAlMn$_{0.3}$	CeAlMn$_{0.5}$	CeAlMn$_{0.7}$
Langmuir	q_m (mg/g)	2.3458	2.6810	2.7863	7.2098	5.5741
	K_L (L/mg)	0.3126	0.0926	0.0566	0.0156	0.0217
	R^2	0.9951	0.6338	0.7822	0.1025	0.3327
Freundlich	K_F (mg/g)	0.6460	0.3554	1.4857	0.1573	0.1550
	n (g/L)	2.2655	1.8854	0.2042	1.2715	1.2625
	R^2	0.9431	0.9007	0.9630	0.8804	0.9412
Temkin	B (kJ/mol)	0.5059	0.5515	0.5126	0.7766	0.6861
	A (L/g)	3.1733	1.1314	0.7713	0.4705	0.5246
	R^2	0.979	0.7204	0.9043	0.6582	0.817

Table 4
Comparative adsorption capacities of MV dye onto various adsorbents

Adsorbents	Adsorption capacity of MV dye (mg/g)	T (°C)	References
CeAl	25.28	25	[7]
Soil silver nanocomposite	1.92	30	[38]
Mansonia wood sawdust	16.11	26	[39]
Siliceous material	20.0	30	[40]
Banana peel	12.20	30	[41]
Orange peel	11.50	30	[41]
HNT-Fe_3O_4 composite	20.04	25	[42]
CeAl	2.35	25	Present study

adsorbing MV molecules. This is referred to as sulfur poisoning and it has been widely studied in catalytic reactions. Xiaodong et al. [24] reported that formation of sulfates on the surface of a MnO_x-CeO_2-Al_2O_3 catalyst resulted in a loss of active surface sites, thereby preventing NO_x oxidation. Seo et al. [37] reported that the NO_x adsorption capacity on a lean NO_x trap-selective catalytic reduction (LNT-SCR) catalyst was decreased due to hydrothermal aging and sulfur poisoning. CeAl exhibited a higher capacity for MV adsorption in comparison to soil- silver nanocomposite. Poorer capacities were previously achieved using mansonia wood sawdust, siliceous material, banana and orange peels and a HNT-Fe_2O_4 composite.

3.6. Discussion

Considering the CeAl data of Table 2 and the Langmuir isotherm modeling of this adsorbent, it may be concluded that this mixed oxide is a classic example of an equilibrium being established between monolayer adsorption and desorption of MV dye molecules in an aqueous solution. However the Freundlich and Temkin models also exhibited high R^2 values for CeAl and neither of these models assumes monolayer adsorption. A Langmuir process assumes that, at equilibrium, there is a balance between the rates at which dye molecules are being adsorbed and the rate at which they are desorbing. However, if the dye molecules are unable to desorb there must be other processes at play which limit the adsorption of MV dye onto the mixed oxides. Indeed, the results of equilibrium isotherm modeling did not suggest that the classic Langmuir model was appropriate for the other adsorbent materials. The R^2 values obtained for all oxides containing manganese ranged from 0.1 to 0.7, with an average of only 0.46. So, even though the Langmuir model may be appropriate for CeAl, it was clearly inappropriate for all the other mixed oxides investigated.

The equilibrium data of Table 2 is also surprising in that none of the MV dye uptake levels for any of the mixed oxides shows signs of saturation. Considering the CeAl data shown in Table 2 and Fig. 7 as representative of all of the mixed oxides, for the 5 mg/L initial dye concentration, there is an 80% uptake at equilibrium with the amount of adsorbed MV dye being 0.1 g. So, the MV dye solution was not fully depleted. However, the adsorbent is also not saturated because for the 50 mg/L initial dye concentration, more than 0.8 mg of MV dye was adsorbed. Saturation would be expected if, for example, the number of sites available for MV dye adsorption was insufficient to adsorb all of the dye from solution before an equilibrium between adsorbent and solution was established. If this had occurred, some of the curves in Fig. 7 should have shown saturation at higher MV dye concentrations. The possible that the "poisoning" effect of sulfur in the mixed oxide samples reduced the number of sites initially available and thus made it even more likely that saturation would have been observed.

It is likely that there are other mechanisms at play, even in the case where CeAl was the adsorbent material. This yielded similar steady-state solutions as the other equilibrium models investigated. These mechanisms can be investigated by incorporating them in kinetic rate equations and computing both their time-dependent and steady-state solutions. Some preliminary work has been done on the possibility that other mechanisms are important. It appears that the experimental results obtained for all the mixed oxide adsorbents might be accounted for by a model that includes oxide particle agglomeration. Agglomeration removes sites progressively, thus limiting the uptake of dye depending on the rate at which MV dye is adsorbed relative to the rate at which sites are lost by particle agglomeration. This kinetic modeling work is ongoing because a number of other possible mechanisms, such as fixed or progressive poisoning of adsorption sites, must be investigated for their consistency with the data.

It is clear that the details of the interaction between adsorbent and adsorbate must be established before a full understanding of this material system in its application to MV dye removal can be achieved. The significance of this understanding is that it will point the way to achieving higher levels of MV dye uptake by this class of materials.

4. Conclusions

CeAl and $CeAlMn_x$ (x = 0.1, 0.3, 0.5 and 0.7) mixed oxides were successfully prepared via a co-precipitation method. The adsorbents were characterized using XRD, FT-IR, UV-vis DRS, SEM and EDX. It was found that the oxides had a highly porous structure exhibiting the cubic fluorite structure of CeO_2 and they appear to be homogeneous. Adsorption experiments showed that the removal of MV dye by CeAl and $CeAlMn_x$ with x = 0.1 and 0.3 attained equilibrium after 60 min, which was faster than those for x = 0.5 and 0.7. Increasing the initial dye concentration increased adsorption capacity. The adsorption behavior of methyl violet adsorption onto CeAl was found to follow the Langmuir isotherm, providing a maximum monolayer adsorptive capacity of 2.35 mg/g. The adsorption of methyl violet dye onto the $CeAlMn_x$ compounds was better described by the Freundlich isotherm. In summary, the Langmuir adsorption/desorption model doesn't appear to fit all the data presented in this work. Efforts to determine the relevance of other processes by performing kinetic analyses which included processes such as particle agglomeration are ongoing.

Acknowledgments

The authors would like to acknowledge the Department of Chemistry, the Faculty of Science and the Research and Development Institute at Udon Thani Rajabhat University, Thailand for their financial support of this research. Many thanks to Professor Dr. Jeffrey C. Nash from the School of Graduate Studies and Assoc. Prof. Dr. Brian Francis Usher from the Department of Physics, Udon Thani Rajabhat University for their assistance in proof reading this manuscript.

References

[1] P. Monash, G. Pugazhenthi, Adsorption of crystal violet dye from aqueous solution using mesoporous materials synthesized at room temperature, Adsorption, 15 (2009) 390–405.

[2] A. Vachálková, L. Novotný, M. Blesová, Polarographic reduction of some triphenylmethane dyes and their potential carcinogenic activity, Neoplasma, 43 (1996) 113–117.

[3] S.M. Doke, G.D. Yadav, Novelties of combustion synthesized titania ultrafiltration membrane in efficient removal of methylene blue dye from aqueous effluent, Chemosphere, 117 (2014) 760–765.

[4] G. Muthuraman, Extractive removal of astacryl blue BG and astacryl golden yellow dyes from aqueous solutions by liquid-liquid extraction, Desalination, 277 (2011) 308–312.

[5] J. Basiri Parsa, S. Hagh Negahdar, Treatment of wastewater containing Acid Blue 92 dye by advanced ozone-based oxidation methods, Sep. Purif. Technol., 98 (2012) 315–320.

[6] A. Asghar, A.A.A. Abdul Raman, W.M.A. Wan Daud, Advanced oxidation processes for *in-situ* production of hydrogen peroxide/hydroxyl radical for textile wastewater treatment: a review, J. Clean. Prod., 87 (2015) 826–836.

[7] P. Phatai, C.M. Futalan, Removal of methyl violet dye by adsorption onto mesoporous mixed oxides of cerium and aluminum, Desal. Wat. Treat., 57 (2016) 8884–8893.

[8] P. Phatai, S. Utara, N. Hatthapanit, Removal of methyl violet by adsorption onto activated carbon derived from coffee residues, Adv. Mater. Res., 864–867 (2014) 710–714.

[9] F. Deniz, Adsorption properties of low-cost biomaterial derived from *Prunus amygdalus* L. for dye removal from water, Sci. World J., 2013 (2013) 1–8.

[10] R.S. Raveendra, P.A. Prashanth, R. Hari Krishna, N.P. Bhagya, B.M. Nagabhushana, H. Raja Naika, K. Lingaraju, H. Nagabhushana, B. Daruka Prasad, Synthesis, structural characterization of nano $ZnTiO_3$ ceramic: an effective azo dye adsorbent and antibacterial agent, J. Asian Ceram. Soc., 2 (2014) 357–365.

[11] S. Rangabhashiyam, N. Anu, N. Selvaraju, Sequestration of dye from textile industry wastewater using agricultural waste products as adsorbents, J. Environ. Chem. Eng., 1 (2013) 629–641.

[12] V.V. Basava Rao, S. Ram Mohan Rao, Adsorption studies on treatment of textile dyeing industrial effluent by flyash, Chem. Eng. J., 116 (2006) 77–84.

[13] M. Roulia, A.A. Vassiliadis, Sorption characterization of a cationic dye retained by clays and perlite, Microporous Mesoporous Mater., 116 (2008) 732–740.

[14] A. Mahapatra, B.G. Mishra, G. Hota, Adsorptive removal of Congo red dye from wastewater by mixed iron oxide-alumina nanocomposites, Ceram. Int., 39 (2013) 5443–5451.

[15] R. Shukla, G. Madras, Facile synthesis of aluminum cobalt oxide for dye adsorption, J. Environ. Chem. Eng., 2 (2014) 2259–2268.

[16] A-N. Chowdhurry, A. Rahim, Y.J. Ferdosi, Md. Shafiul Azam, M. Mufazzal Hossain, Cobalt-nickel mixed oxide surface: a promising adsorbent for the removal of PR dye from water, Appl. Surf. Sci., 256 (2010) 3718–3724.

[17] K. Biswas, K. Gupta, U.C. Ghosh, Adsorption of fluoride by hydrous iron (III)-tin (IV) bimetal mixed oxide from the aqueous solutions, Chem. Eng. J., 149 (2009) 196–206.

[18] C. Klett, A. Barry, I. Balti, P. Lelli, F. Schoenstein, N. Jouini, Nickel doped zinc oxide as a potential sorbent for decolorization of specific dyes, methyl orange and tartrazine by adsorption process, J. Environ. Chem. Eng., 2 (2014) 914–926.

[19] M. Szlachta, N. Chubar, The application of Fe-Mn hydrous oxides based adsorbent for removing selenium species from water, Chem. Eng. J., 217 (2013) 159–168.

[20] K. Biswas, K. Gupta, A. Goswami, U.C. Ghosh, Fluoride removal efficiency from aqueous solution by synthetic iron (III)-aluminum (III)-chromium (III) ternary mixed oxide, Desalination, 255 (2009) 44–51.

[21] X. Wu, Y. Zhang, X. Dou, M. Yang, Fluoride removal performance of a novel Fe–Al–Ce trimetal oxide adsorbent, Chemosphere, 69 (2007) 1758–1764.

[22] M. Chen, Y. Zhu, X. Zheng, A novel material of $Ce_{0.7}Zr_{0.3}Ba_{0.1}O_{2.1}$: synthesis, characterization and its catalytic performance for CO oxidation, Mater. Chem. Phys., 92 (2005) 43–47.

[23] G. Qi, W. Li, NO oxidation to NO_2 over manganese-cerium mixed oxides, Catal. Today, 258 (2015) 205–213.

[24] W. Xiaodong, L. Hyeing-Ryeol, L. Shuang, W. Duan, Sulfur poisoning and regeneration of MnO_x-CeO_2-Al_2O_3 catalyst for soot oxidation, J. Rare Earth, 30 (2012) 659–664.

[25] B.P. Dhonge, T. Mathews, S.T. Sundari, C. Thinaharan, M. Kamruddin, S. Dash, A.K. Tyagi, Spray pyrolytic deposition of transparent aluminum oxide (Al_2O_3) films, Appl. Surf. Sci., 258 (2011) 1091–1096.

[26] M. Akgűl, A. Karabakan, Promote dye adsorption performance over desilicated natural zeolite, Microporous Mesoporous Mater., 145 (2011) 157–164.

[27] G.R. Rao, B.G. Mishra, A comparative UV-vis-diffuse reflectance study on the location and interaction of cerium ions in Al- and Zr-pillared montmorillonite clays, Mater. Chem. Phys., 89 (2005) 110–115.

[28] Z. Li, L. Fudong, Y. Yunbo, L. Yongchun, Z. Changbin, H. Hong, Effects of adding CeO_2 to Ag/Al_2O_3 catalyst for ammonia oxidation at low temperatures, Chin. J. Catal., 32 (2011) 727–735.

[29] M. Zabilskiy, B. Erjavec, P. Djinovic, A. Pintar, Ordered mesoporous CuO-CeO_2 mixed oxides as an effective catalyst for N_2O decomposition, Chem. Eng. J., 254 (2014) 153–162.

[30] L. Wang, J. Li, Y. Wang, L. Zhao, Q. Jiang, Adsorption capacity for Congo red on nanocrystalline MFe_2O_4 (M = Mn, Fe, Co, Ni) spinel ferrites, Chem. Eng. J., 181–182 (2012) 72–79.

[31] R. Liu, B. Zhang, D. Mei, H. Zhang, J. Liu, Adsorption of methyl violet from aqueous solution by halloysite nanotubes, Desalination, 268 (2011) 111–116.

[32] M. Alshabanat, G. Alsenani, R. Almufarij, Removal of crystal violet dye from aqueous solution onto date palm fiber by adsorption technique, J. Chem., 2013 (2013) 1–6.

[33] K. Elass, A. Laachach, A. Alaoui, M. Azzi, Removal of methyl violet from aqueous solution using a stevensite-rich clay from Morocco, Appl. Clay Sci., 54 (2011) 90–96.

[34] F. Del Rey-Bueno, J. Romero-Carballo, E. Villafranca-Sanchez, A. Garcia-Rodriguez, E.N. Sebastian-Pardo, Adsorption of ammonia over halloysite activated at different temperatures, Mater. Chem. Phys., 21 (1989) 67–84.

[35] I.A.W. Tan, A.L. Ahmad, B.H. Hameed, Adsorption of basic dye on high-surface-area activated carbon prepared from coconut husk: equilibrium kinetic and thermodynamic studies, J. Hazard. Mater., 154 (2008) 337–346.

[36] K.M. Parida, S. Sahu, K.H. Reddy, P.C. Sahoo, A kinetic, thermodynamic and mechanistic approach toward adsorption of methylene blue over waste-washed manganese nodule leached residues, Ind. Eng. Chem. Res., 50 (2011) 843–848.

[37] W-K. Seo, H. Kim, B. Choi, M.T. Lim, C-H. Lee, C-B. Lee, De-NO_x characteristics of a combined system of LNT and SCR catalysts according to hydrothermal aging and sulfur poisoning, Catal. Today, 164 (2011) 507–541.

[38] M.K., Satapathy, P. Das, Optimization of crystal violet dye removal using novel soil-silver nanocomposite as nanoadsorbent using response surface methodology, J. Environ. Chem. Eng., 2 (2014) 708–714.

[39] A.E. Ofomaja, Kinetic study and sorption mechanism of methylene blue and methyl violet onto mansonia (*Mansonia altissima*) wood sawdust, Chem. Eng. J., 143 (2008) 85–95.

[40] J.M. Gómez, J. Galan, A. Rodríguez, G.M. Walker, Dye adsorption onto mesoporous materials: pH influence, kinetics and equilibrium in buffered and saline media, J. Environ. Manage., 146 (2014) 355–361.

[41] G. Annadurai, R.S. Juang, D.J. Lee, Use of cellulose-based wastes for adsorption of dyes from aqueous solutions, J. Hazard. Mater., 92 (2002) 263–274.

[42] L.R. Bonetto, F. Ferrarini, C. de Marco, J.S. Crespo, R. Guégan, M. Giovanela, Removal of methyl violet 2B dye from aqueous solution using a magnetic composite as an adsorbent, J. Water Process Eng., 6 (2015) 11–20.